

Reprinted from

JAPANESE JOURNAL OF
**APPLIED
PHYSICS**

REGULAR PAPER

**Estimation of Scatterer Diameter by Normalized Power Spectrum of High-Frequency
Ultrasonic RF Echo for Assessment of Red Blood Cell Aggregation**

Taku Fukushima, Hideyuki Hasegawa, and Hiroshi Kanai

Jpn. J. Appl. Phys. **50** (2011) 07HF02

Estimation of Scatterer Diameter by Normalized Power Spectrum of High-Frequency Ultrasonic RF Echo for Assessment of Red Blood Cell Aggregation

Taku Fukushima¹, Hideyuki Hasegawa^{2,1}, and Hiroshi Kanai^{1,2*}

¹Graduate School of Engineering, Tohoku University, Sendai 980-8579, Japan

²Graduate School of Biomedical Engineering, Tohoku University, Sendai 980-8579, Japan

Received December 13, 2010; accepted March 1, 2011; published online July 20, 2011

Red blood cell (RBC) aggregation, as one of the determinants of blood viscosity, plays an important role in blood rheology, including the condition of blood. RBC aggregation is induced by the adhesion of RBCs when the electrostatic repulsion between RBCs weakens owing to increases in protein and saturated fatty acid levels in blood, excessive RBC aggregation leads to various circulatory diseases. This study was conducted to establish a noninvasive quantitative method for assessment of RBC aggregation. The power spectrum of ultrasonic RF echoes from nonaggregating RBCs, which shows the frequency property of scattering, exhibits Rayleigh behavior. On the other hand, ultrasonic RF echoes from aggregating RBCs contain the components of reflection, which have no frequency dependence. By dividing the measured power spectrum of echoes from RBCs in the lumen by that of echoes from a posterior wall of the vein in the dorsum manus, the attenuation property of the propagating medium and the frequency responses of transmitting and receiving transducers are removed from the former spectrum. RBC aggregation was assessed by the diameter of a scatterer, which was estimated by minimizing the square difference between the measured normalized power spectrum and the theoretical power spectrum. In this study, spherical scatterers with diameters of 5, 11, 15, and 30 μm were measured in basic experiments. The estimated scatterer diameters were close to the actual diameters. Furthermore, the transient change of the scatterer diameters were measured in an *in vivo* experiment with respect to a 24-year-old healthy male during the avascularization using a cuff. The estimated diameters (12–22 μm) of RBCs during avascularization were larger than the diameters (4–8 μm) at rest and after recirculation. These results show the possibility of the use of the proposed method for noninvasive assessment of RBC aggregation.

© 2011 The Japan Society of Applied Physics

1. Introduction

Medical ultrasound is clinically used to make a diagnosis for various organs, and it can be repeatedly employed to confirm time-dependent changes because it is noninvasive and patients have less stress. For diagnosis of atherosclerosis, ultrasound imaging is widely used for morphological observation of the arterial wall. Furthermore, methods for evaluating the viscoelasticity of the arterial wall have recently been developed.^{1,2)}

As well as the morphology and viscoelasticity of the arterial wall, the condition of blood is also a useful marker for the diagnosis of atherosclerosis.^{3,4)} However, conventional ultrasonic images cannot be applied to evaluate the condition of blood because red blood cells (RBCs), which are the main components of blood, are much smaller than the wavelength of the ultrasound and the difference in acoustic impedance between blood plasma and RBCs is very small.

RBC aggregation, as one of the determinants of blood viscosity, plays an important role in the condition of blood.^{3,5)} The tunica adventitia of healthy RBCs is charged with negative electricity, which impedes RBC adherence by electrostatic repulsion.⁶⁾ However, due to the increase in the adhesive force of high-molecular substances such as protein, saturated fatty acid, and cholesterol in blood serum, the force of electrostatic repulsion between RBCs is weakened. As a result, RBC aggregation easily occurs.⁷⁾

RBCs play a role to carry oxygen and nutritive components to all parts of the body. RBC aggregation degrades such ability of RBCs.⁸⁾ Therefore, excessive RBC aggregation becomes a factor for diabetes and hyperlipidemia because less protein and lipid are chronically carried for each organ.^{9,10)} In addition, RBC aggregation increases blood viscosity⁷⁾ and, therefore, the excessive RBC aggregation also becomes a factor for thrombosis and atherosclerosis

because the increase of blood viscosity leads to the morphological change of vascular wall such as the endothelial dysfunction and the characteristic change of smooth muscle.^{11,12)} Consequently, assessment of RBC aggregation is essential.

The microchannel array flow analyzer (MC-FAN) method is a recently developed technique for evaluating the condition of blood by observation of whether red blood cells pass through gaps in silicon substrates simulating blood capillaries.¹³⁾ However, this method is not quantitative. Furthermore, the blood is collected with a syringe and measured after administration of anticoagulant, i.e., invasive, results being influenced by such collection and the amount of administered anticoagulant. Many studies on assessment of RBC aggregation in various organs have been reported. Shung *et al.* observed blood echogenicity variation during the cardiac cycle.^{14,15)} Lizzi *et al.* showed that sizes of scatterers in tissue could be estimated from the spectral slope.¹⁸⁾ However, these methods and studies are invasive due to collection of blood as well as employment of the MC-FAN method. Furthermore, Cloutier *et al.* estimated blood structure parameters relating to scatterer size, attenuation, and scattering cross section of the backscattering coefficient in *in vivo* measurement.^{16,17)} However, the size of aggregated RBCs have not yet been estimated in *in vivo* measurements. The purpose of the present study was to establish a noninvasive quantitative method for assessment of RBC aggregation.

In our previous study,⁴⁾ RBC aggregation was assessed by estimating the spectral slope. However, the calculation of the spectral slope requires application of a high-pass filter which decreases the estimation accuracy of scatterer diameter and increases the influence of random noise including echoes. Furthermore, the attenuation property of the propagation path was not completely removed in the estimation of the spectral slope. In addition, although some researchers have estimated scatterer size and the attenuation property for normalization,^{18,19)} noninvasive estimation of scatterer

*E-mail address: kanai@ecei.tohoku.ac.jp

diameter by removing the attenuation property of the propagating medium for normalization is difficult due to inhomogeneous tissues with unknown attenuation properties. For dealing with this problem, we improved the method for normalization of the measured power spectrum and developed a new method to estimate scatterer diameter from the normalized power spectrum.

2. Principles

2.1 Theoretical power spectrum of scattered echoes

An RBC is a very small ultrasonic scatterer whose diameter is 8 μm at most. In addition, the difference between acoustic impedance of blood plasma and that of an RBC is very small; thus, the amplitudes of scattered RF echoes are very small. Therefore, the power spectrum of the echoes from RBCs is calculated using the fast Fourier transform (FFT) to evaluate in the frequency domain because the scattering properties of RF echoes are various, corresponding to scatterer size. In addition, it was assumed that the diameter of a scatterer increases depending on the degree of RBC aggregation.

In the present study, a scatterer was modeled by placing an infinite number of infinitesimal point sources on the surface of the scatterer. When a plane wave insonifies the scatterer, the theoretical power spectrum $Q(ka)/\pi a^2$ of the scattered echo is given by²⁰⁾

$$\frac{Q(ka)}{\pi a^2} = 4 \sum_{n=0}^{\infty} \frac{2n+1}{(ka)^2} \sin^2[\delta'_n(ka)], \quad (1)$$

where $Q(ka)$ is the scattering cross section, k is the wave number, a is the radius of the scatterer, n is the number of point sources on the surface of the scatterer, and $\delta'_n(ka)$ is the derivation of the phase difference between the incident wave and the scattered wave.

Figure 1 shows the theoretical power spectrum $Q(ka)/\pi a^2$ as a function of ka . Furthermore, the power spectrum $Q(ka)/\pi a^2$ is also given as a function of frequency (f) and scatterer radius (a) by transforming $ka = 2\pi(a/\lambda) = (2\pi/c)fa$, where c is the acoustic velocity. Therefore, logarithmic theoretical power spectra $\log_{10} Q(ka)/\pi a^2$ at different scatterer radii as a function of frequency (f) are shown in Fig. 2.

2.2 Normalization in power spectrum

The power spectrum of ultrasonic RF echoes from nonaggregating RBCs exhibits Rayleigh behavior.^{21,22)} It is well known that the power spectrum $P_s(f)$ of the scattered wave is proportional to the fourth power of frequency. On the other hand, ultrasonic RF echoes from aggregating RBCs contain the components of reflection, which have no frequency dependence. Therefore, the spectral slope decreases when scatterer size increases and the components of reflection are included in the echoes.²³⁾

The measured spectrum $Z_s(f)$ of the received ultrasonic echo signal $e_s(t)$ contains the scattering property $S(f)$ from scatterers, the frequency response $G(f)$ of transmitting and receiving transducers, and the attenuation property $A_1(f)$ of the propagating medium. In summary, the measured spectrum $Z_s(f)$ is given by

$$Z_s(f) = S(f)G(f)A_1(f) \cdot X(f), \quad (2)$$

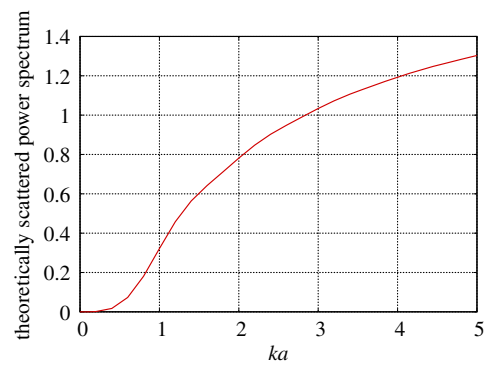


Fig. 1. (Color online) Theoretical power spectrum $Q(ka)/\pi a^2$ of a scattered echo.

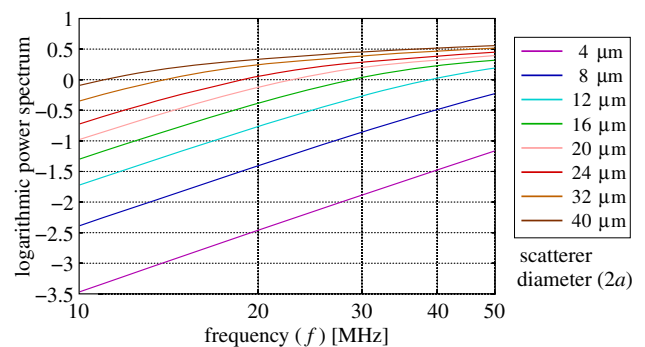


Fig. 2. (Color online) Logarithmic theoretical power spectrum $\log_{10} Q(ka)/\pi a^2$ with constant values in each scatterer diameter ($2a$).

where $X(f)$ is the spectrum of the transmitted signal. The normalization of the power spectrum has been introduced by some researchers.^{24,25)} Cloutier *et al.* removed the frequency response $G(f)$ of the transmitting and receiving transducer.¹⁶⁾ However, the attenuation property $A_1(f)$ of the propagation medium is difficult to remove under *in vivo* conditions because the propagation medium in *in vivo* measurements is inhomogeneous tissue with unknown attenuation properties.

Therefore, in the present study, the power spectrum $P_r(f)$ of ultrasonic RF echoes from the posterior wall of the vein was used for normalization because the propagation media in the measurements of the posterior wall and in the measurements of RBCs in the lumen of the vein are similar so that not only the frequency response $G(f)$ of the transducer but also the attenuation property $A_1(f)$ of the propagation medium can be removed. Therefore, normalization is performed as below:

$$\begin{aligned} 10 \log_{10} \frac{P_s(f)}{P_r(f)} &= 10 \log_{10} \frac{|Z_s(f)|^2}{|Z_r(f)|^2} \\ &= 10 \log_{10} \frac{|S(f)G(f)A_1(f) \cdot X(f)|^2}{|R(f)G(f)A_2(f) \cdot X(f)|^2} \\ &\approx 10 \log_{10} \frac{|S(f)|^2}{|R(f)|^2}, \end{aligned} \quad (3)$$

where $R(f)$ is the reflecting property and $A_2(f)$ is the attenuation property of the propagating medium in the measurement of echoes from the posterior wall of the vein.

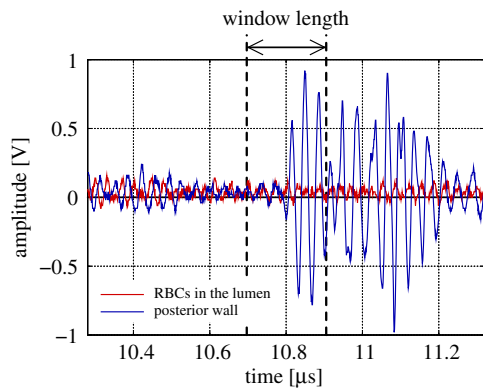


Fig. 3. (Color online) RF echoes from RBCs in the lumen of the vein and the posterior wall obtained by compressing the vein.

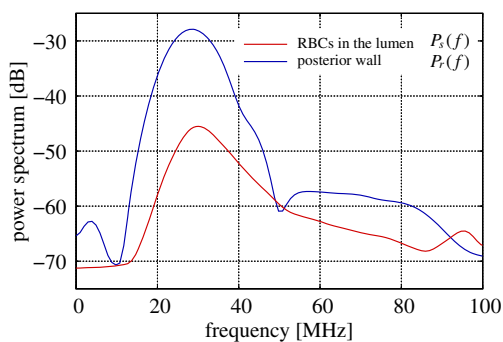


Fig. 4. (Color online) Power spectra of the ultrasound echoes reflected from the posterior wall and scattered from RBCs in the lumen.

Figure 3 shows RF echoes reflected by the posterior wall (blue line) and scattered from RBCs (red line) in the lumen. RF echoes reflected by the posterior wall include echoes from the tissues under the posterior wall and RBCs in the lumen. Such undesirable echoes were suppressed by applying a Hanning window centered at the central time of an echo from the posterior wall (10.8 μs) before the Fourier transform was performed. Window length was 0.256 μs , which corresponds to the pulse duration of the echo from the posterior wall. Figure 4 shows the power spectrum $P_r(f)$ from the posterior wall and the power spectrum $P_s(f)$ from RBCs in the lumen. Each power spectrum in Fig. 4 was obtained by averaging 1000 power spectra of RF echoes to reduce the influences of dips originating from the interference of particular echoes scattered from RBCs.

2.3 Estimation method of scatterer size using weighting function

In the present study, scatterer size was estimated by determining the theoretical power spectrum $\log_{10} Q(ka)/\pi a^2$, which minimized the difference between the measured normalized power spectrum $\log_{10} P_s(f)/P_r(f)$ and theoretical power spectrum $\log_{10} Q(ka)/\pi a^2$ shown in Fig. 2. Let us define the square difference (α) between the measured normalized power spectrum $\log_{10} P_s(f)/P_r(f)$ and the theoretical power spectrum $\log_{10} Q(ka)/\pi a^2$ as follows:

$$\alpha = \frac{1}{N} \sum_{k=0}^{N-1} w(f_k)^2 \{y(f_k) - [\hat{y}(f_k, 2a) + b]\}^2, \quad (4)$$

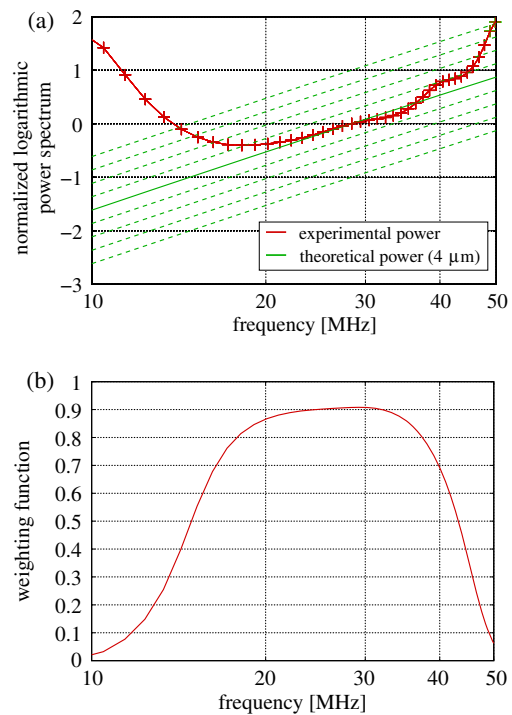


Fig. 5. (Color online) (a) Measured normalized logarithmic power spectrum $\log_{10} P_s(f)/P_r(f)$ and logarithmic theoretical power spectrum $\log_{10} Q(ka)/\pi a^2$ shifted in the vertical direction at scatterer diameter of 4 μm . (b) Weighting function $w(f_k)$ obtained from MSCF among the ultrasonic echoes scattered from RBCs in the lumen using same echoes as Fig. 5(a).

where $y(f_k)$ is the measured normalized logarithmic power spectrum $\log_{10} P_s(f_k)/P_r(f_k)$ at a frequency of f_k , $\hat{y}(f_k)$ is the logarithmic theoretical power spectrum $\log_{10} Q(ka)/\pi a^2$, f_k is the discrete frequency, b is the intercept of the theoretical power spectrum, and $w(f_k)$ is the weighting function.

In this study, by considering the signal-to-noise ratio (SNR) of the echo at each discrete frequency, the weighting function $w(f_k)$ was defined by the magnitude-squared coherence function (MSCF) $|\gamma(f_k)|^2$ as follows:²⁶⁾

$$w(f_k) = |\gamma(f_k)|^2 = \frac{|E_n[Y_n^*(f_k)Y_{n+1}(f_k)]|^2}{E_n[|Y_n(f_k)|^2] \cdot E_n[|Y_{n+1}(f_k)|^2]}, \quad (5)$$

where $Y_n(f_k)$ is power spectrum in each beam from RBCs in the lumen, $E_n[\cdot]$ is the averaging operation for the frames, $*$ is the complex conjugate, and n is the frame number.

Figure 5(a) shows measured normalized logarithmic power spectrum $\log_{10} P_s(f_k)/P_r(f_k)$ (red solid line) and logarithmic theoretical power spectrum $\log_{10} Q(ka)/\pi a^2$ (green solid and dashed lines) at a scatterer radius a of 4 μm , and Fig. 5(b) shows the weighting function $w(f_k)$ obtained from the same ultrasonic echoes shown in Fig. 5(a), which were scattered from RBCs in the lumen. In this study, we define the weighting function $w(f_k)$ obtained from MSCF among received RF echoes from RBCs of the lumen to consider the SNR of echoes from RBCs, which is the signal of interest. As shown in Fig. 5(a), for each size (diameter) of scatterers, the difference between the measured and theoretical power spectrum was minimized by changing the intercept (b) of the theoretical power spectrum. As a consequence, scatterer radius is estimated to be the size giving the smallest sum of the square difference α .

Table I. Particle diameters, properties, and polymer materials of each microsphere.

	Particle diameter mean \pm SD (μm)	Specific gravity	Volume fraction (%)	Polymer material
(1)	5 ± 2	1.10	0.0910	Acrylic nitrile, vinylidene chloride
(2)	11 ± 3	1.00	0.1000	Acrylic nitrile
(3)	15 ± 5	1.11	0.0901	Acrylic nitrile, vinylidene chloride
(4)	30 ± 10	1.00	0.1000	Acrylic nitrile

3. Basic Experiments Using Microspheres

Ultrasound diagnostic equipment (Tomey UD-1000) equipped with a mechanical scan probe at a center frequency f_0 of 40 MHz (wavelength is about $40 \mu\text{m}$) was used for acquiring ultrasonic echo signals. The RF echoes were acquired at a sampling frequency of 1 GHz at a 8-bit resolution by an oscilloscope (Tektronix DPO7054), and their power spectra were obtained by applying the fast Fourier transform with a Hanning window of $0.256 \mu\text{s}$ in length. In the present study, 768 zero points were added so that signal length for Fourier analysis became $1.024 \mu\text{s}$ to improve the frequency resolution.

Table I shows the sizes and properties of the measured microspheres. The shells of microspheres (1) and (3) were made of copolymer including acrylic nitrile and vinylidene chloride with Cl_2 , and microspheres (2) and (4) were made of copolymer including acrylic nitrile without Cl_2 . In addition, the liquid hydrocarbon is included inside each microsphere. Microspheres of different sizes, which were mixed with water at a density of 1.00 g/l , simulated nonaggregated RBCs and aggregated RBCs. This density is lower than that of RBCs in actual blood to prevent the concentration of microspheres.

In addition, RF echoes from a silicone plate, which was used as a reflector, were measured with microspheres in the water at the same density as the measurement of RF echoes from the microspheres. Influences of the difference between acoustic impedances of microspheres and RBCs was not considered in the present study.

Figure 6(a) shows the averaged power spectrum $P_s(f)$ of echoes from each microsphere. Figure 6(b) shows the averaged power spectrum $P_r(f)$ of echoes from the silicone plate in the water with each microsphere. The numbers correspond to the microsphere numbers in Table I. In the basic experiments, microspheres with and without Cl_2 were used as a scatterer. Therefore, the acoustic properties may be varied by adding Cl_2 . Actually, as shown in Fig. 6(a), the magnitude of the power spectrum $P_s(f)$ of echoes from a larger sphere is not always greater than that from a smaller sphere, which suggests that the acoustic impedance may be varied by Cl_2 . However, in the present study, scatterer diameters are not estimated from the magnitude of the power spectra $P_s(f)$, but from the frequency properties corresponding to the slope of the normalized power spectrum $\log_{10} P_s(f)/P_r(f)$, so that the estimation of the scatterer diameters is less influenced by the existence of Cl_2 in the shells. Furthermore, to acquire echoes from various

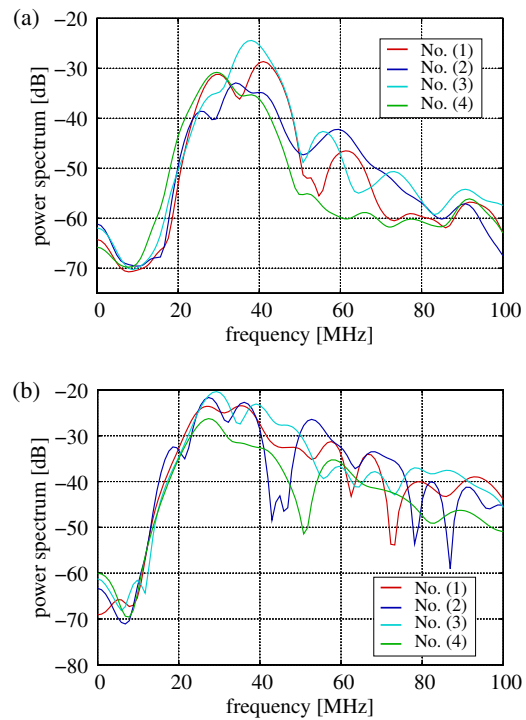


Fig. 6. (Color online) (a) Power spectra $P_s(f)$ of the ultrasonic echoes from the microspheres (1)–(4) in Table I. (b) Power spectra $P_r(f)$ of the ultrasonic echoes from the silicone plate with microspheres (1)–(4) in the water.

statistically different spatial distribution of spheres, RF echoes from the microspheres were measured by manually stirring microspheres to keep a certain flow rate.

Figure 7(a) shows the logarithmic normalized power spectra $\log_{10} P_s(f)/P_r(f)$ (solid line) and the logarithmic theoretical power spectra $\log_{10} Q(ka)/\pi a^2$ (dashed line) corresponding to the estimated scatterer diameters. Figure 7(b) shows the weighting functions $w(f_k)$ for each microsphere. As shown in Fig. 7, the normalized power spectra $\log_{10} P_s(f)/P_r(f)$ show high values at the frequency range around 10 MHz. As shown in Figs. 6(a) and 6(b), the power spectra $P_s(f)$, $P_r(f)$ of echoes from the microsphere and the silicone plate show similar and low magnitude in a frequency range less than 10 MHz because RF echoes hardly contain such frequency components. Therefore, the normalized power spectrum $\log_{10} P_s(f)/P_r(f)$ shows around 0 dB and the weighting function $w(f_k)$ obtained from the echoes scattered from microspheres shows low values at the frequency range less than 10 MHz due to low SNRs. However, the power spectrum $P_r(f)$ of echoes from the silicone plate shows high magnitudes compared with the power spectrum $P_s(f)$ of echoes from the microsphere in the range from 20 to 40 MHz, which corresponds to the width at half maxima of power spectrum, because the amplitude of the echoes from the silicone plate shows high compared with that of the echoes from the microsphere. Therefore, the normalized power spectrum $\log_{10} P_s(f)/P_r(f)$ shows negative values. Consequently, the normalized power spectrum $\log_{10} P_s(f)/P_r(f)$, which calculated by dividing the power spectrum $P_r(f)$ of the echoes obtained from the silicone plate by the power spectrum $P_s(f)$ of the echoes obtained from microsphere, show high values at the frequency range less than 10 MHz.

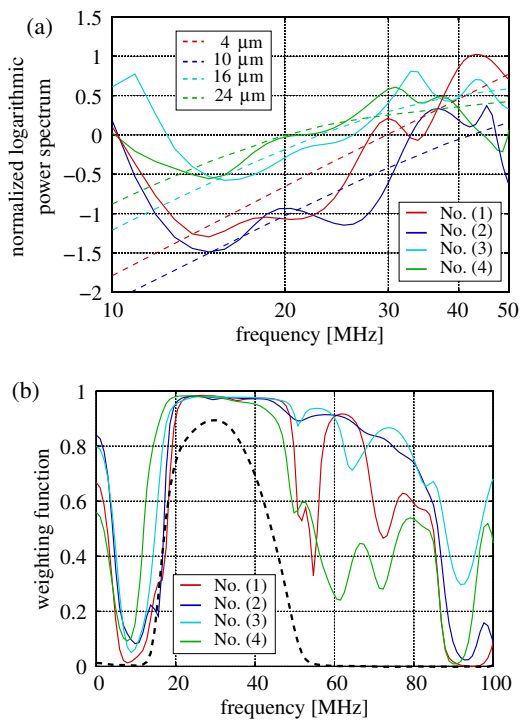


Fig. 7. (Color online) (a) Normalized power spectra $P_s(f)/P_r(f)$ of microspheres (1)–(4) in Table I and logarithmic theoretical power spectra $\log_{10} Q(ka)/\pi a^2$ corresponding to the estimated scatterer diameters. (b) Weighting function $w(f_k)$ obtained from MSCF among the ultrasound echoes scattered from microspheres (1)–(4) in Table I (solid line) and scattered from RBCs in the lumen of the vein (dashed line).

As shown in Fig. 7(a), there are large dips in the normalized power spectra $\log_{10} P_s(f)/P_r(f)$. These dips are considered to be occurred by the interference of echoes from the surface and other particular positions such as inside of the silicone plate, which were included in the window for the frequency analysis because the RF echoes reflected from silicone plate are acquired from the same fixed beam.

As shown in Fig. 7(b), the weighting functions are considered to show large values between 50 and 90 MHz due to the influence of the multiple scattering among microspheres caused by strong scattering of microspheres unlike RF echoes from RBCs in the lumen. However, the value of the weighting functions $w(f_k)$ decreased at about 50 MHz in all microspheres. In addition, the frequency range applied for normalization was limited because of using the ultrasonic pulse, which has a finite frequency bandwidth. In the present study, therefore, the normalized power spectrum $\log_{10} P_s(f)/P_r(f)$ in the frequency range from 10 to 50 MHz was used to estimate the scatterer diameters.

The Table II shows the mean and the standard deviation, and the maximum and minimum of the estimated scatterer diameters for ten measurements of each microsphere. Although some of the estimated scatterer diameters were beyond the actual scatterer diameters, as shown in the left-hand column of Table II, estimated scatterer diameters are approximately true values.

4. In vivo Experiments

RBCs in blood do not aggregate in large blood vessels because of high blood shear rate.^{27–29} In this study, to

Table II. Particle diameters and experimental estimated results of each microsphere.

	Particle diameter mean ± SD (μm)	Estimated scatterer diameter mean ± SD (μm)	Maximum and minimum values in the 10 measurements (μm)
(1)	5 ± 2	6.8 ± 3.7	4–14
(2)	11 ± 3	8.7 ± 4.8	4–16
(3)	15 ± 5	15.1 ± 2.9	8–18
(4)	30 ± 10	30.6 ± 7.9	18–40

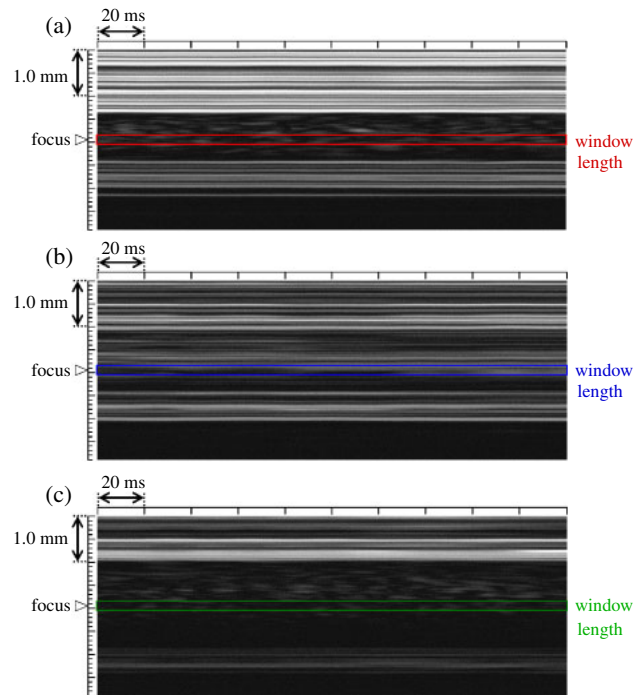


Fig. 8. (Color online) M-mode images of RF echoes from the focal point positioned in the lumen of the vein at the dorsum manus: at rest (a), during avascularization (b), and after recirculation (c).

measure ultrasonic echoes from the blood, a condition which tends to occur in aggregated RBCs, blood flow was stopped by applying pressure with a cuff surrounding the upper arm at 250 mmHg. Ultrasonic echoes were acquired at rest for 2 min, during avascularization for 5 min, and after recirculation for 3 min. Figure 8 shows M-mode images of 1000 RF echoes measured at the same fixed beam from a vein at the dorsum manus of a 24-year-old healthy male. The M-mode images were measured at rest (a), during avascularization (b), and after recirculation (c).

The vein measured in this study had a large diameter of 1 mm and a high blood shear rate, which affected RBC aggregation. Therefore, it was assumed that the RF echoes scattered from nonaggregated RBCs were measured at rest. Furthermore, we measured the change in scatterer diameters caused by the decrease in the blood shear rate due to avascularization using a cuff.

Figure 9(a) shows a M-mode image of the vein. The vein was compressed so that the focal point corresponded to the posterior wall to obtain echoes reflected from the posterior wall for normalization of power spectrum $P_s(f)$ of echoes

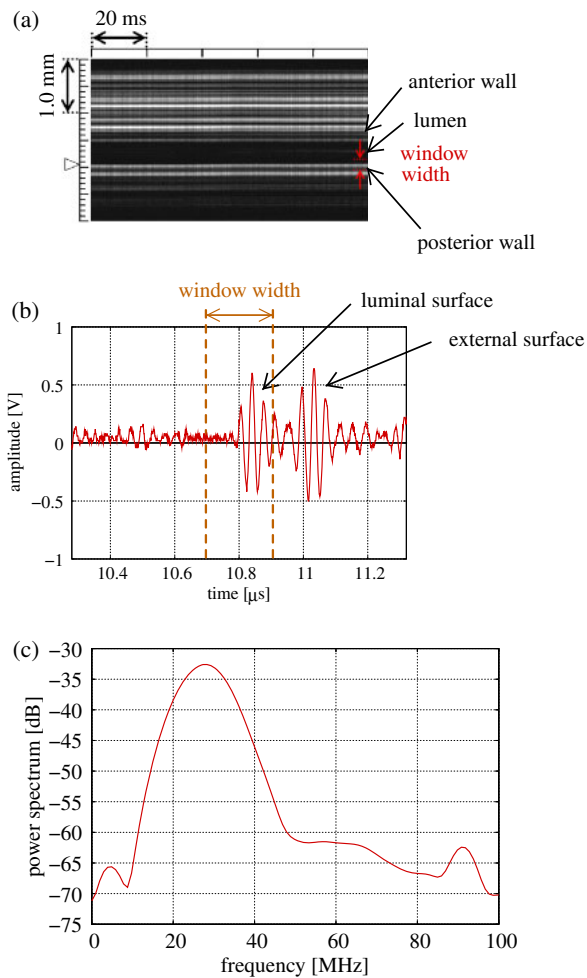


Fig. 9. (Color online) (a) M-mode image of the posterior wall of the vein at the dorsum manus of a 24-year-old male and focal point was placed on the posterior wall. (b) RF echoes from posterior wall of the vein obtained by compressing the vein. (c) Power spectra $P_r(f)$ of the ultrasound echoes reflected from the posterior wall.

from RBCs. Figure 9(b) shows the RF echoes from posterior wall of the vein. Figure 9(c) shows the averaged power spectra $P_r(f)$ of echoes from the posterior wall of the vein at the dorsum manus. In the present study, the window length for applying fast Fourier transform was set at $0.256 \mu\text{s}$, where it roughly corresponds to the duration of the echo from the posterior wall. As shown in Fig. 9(c), the power spectrum $P_r(f)$ from the posterior wall is obtained by echoes from the luminal surface of the posterior wall. On the other hand, when echoes from the luminal and external surfaces are included in the window for frequency analysis, the power spectrum $P_r(f)$ shows dips due to the interference between these echoes.

Figure 10 shows the normalized logarithmic power spectra $\log_{10} P_s(f)/P_r(f)$ (solid line), and the logarithmic theoretical power spectra $\log_{10} Q(ka)/\pi a^2$ (dashed line) corresponding to the estimated scatterer diameters.

Figure 11 shows the transient change of averaged estimated scatterer diameters with standard deviations for three *in vivo* measurements with avascularization. The scatterer diameters at rest and after recirculation were estimated to be $4\text{--}8 \mu\text{m}$, which corresponded to the sizes of nonaggregated RBCs. On the other hand, the scatterer

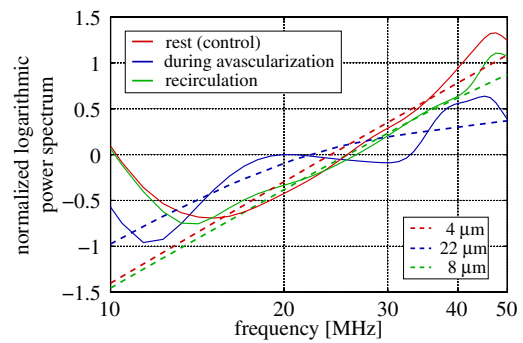


Fig. 10. (Color online) Normalized logarithmic power spectra $\log_{10} P_s(f)/P_r(f)$ and logarithmic theoretical power spectra $\log_{10} Q(ka)/\pi a^2$ corresponding to the estimated scatterer diameters: at rest, during avascularization, and after recirculation.

diameters during avascularization were estimated to be about $12\text{--}22 \mu\text{m}$, which corresponded to the sizes of aggregated RBCs and were greater than those at rest and after recirculation. However, the standard deviations of estimated scatterer diameters during avascularization are large because there would be various sizes of aggregated RBCs. Scatterer sizes due to avascularization were varied and blood flow during avascularization was stopped by applying pressure with a cuff. In addition, RF echoes from the RBCs in the lumen could be different with respect to each measurement due to the displacement of the manus and blood flow. Therefore, it is considered that the estimated scatterer diameters in each measurement are widely different although the power spectrum was obtained by averaging 1000 power spectra of RF echoes.

5. Discussion and Conclusions

From the basic experiments using microspheres, it was shown that the scatterer diameters could be estimated by minimizing the difference between the measured power spectrum $\log_{10} P_s(f)/P_r(f)$ and the theoretical power spectrum $\log_{10} Q(ka)/\pi a^2$.

As shown in Figs. 5(b) and 7(b), the weighting functions $w(f_k)$ are different between basic experiments and *in vivo* experiments. Figure 12(a) shows the M-mode images of RF echoes and an example of the received RF echoes from microsphere (1) in Table I at three different densities: (a) 0.10, (b) 0.50, and (c) 1.00 g/l. As shown in Figs. 12(a) and 12(b), the comet signs are observed in the three M-mode images, which is considered to be caused by the multiple reflection inside each microsphere.

Figure 13(a) shows the averaged power spectra $P_s(f)$ of microsphere (1) in Table I obtained at three different densities of microspheres mixed with water: 1.00, 0.50, and 0.10 g/l. Figure 13(b) shows the weighting function $w(f_k)$ for each density of microsphere. As shown in Fig. 13(a), the power spectrum $P_s(f)$ of echoes from microsphere (1) at the density of 1.00 g/l is influenced by dips, by contrast, the power spectra $P_s(f)$ of echoes from microsphere (1) at the density of 0.10 and 0.50 g/l are less influenced by dips. As a result, dips in the power spectrum are considered to be caused by the interference occurred from a number of microspheres. Therefore, the density of microspheres mixed in the water should be further

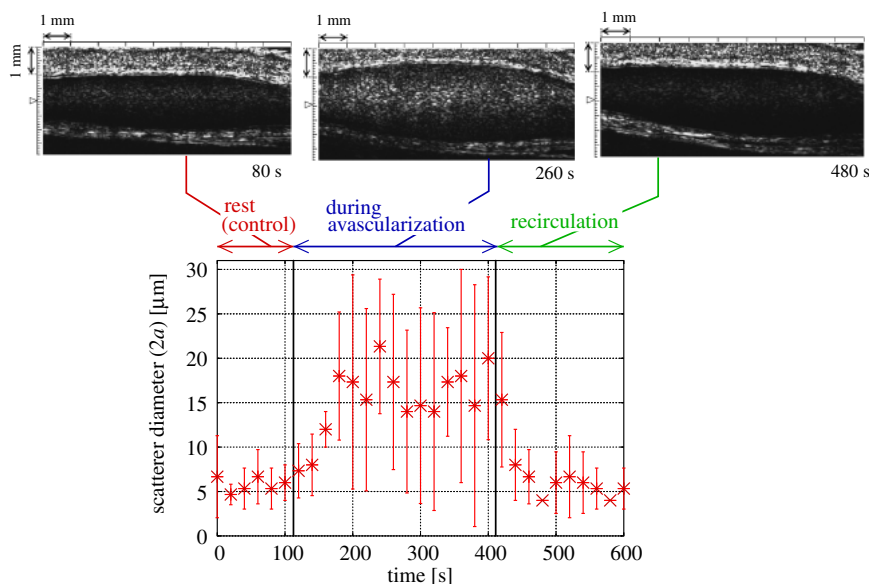


Fig. 11. (Color online) Transient change of averaged estimated scatterer diameters with standard deviations during 10 min obtained by three *in vivo* measurements. B-mode image in each phase of measurement is also shown.

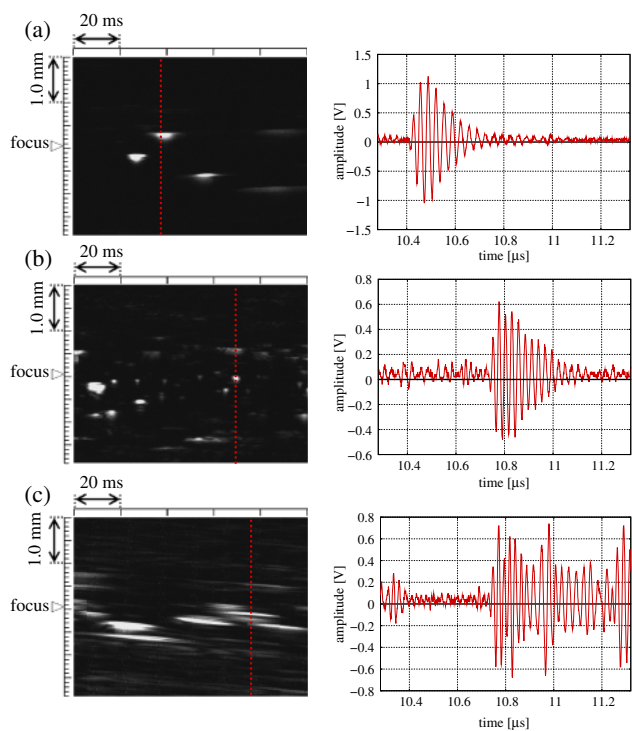


Fig. 12. (Color online) M-mode images of RF echoes and an example of the received RF echoes from microsphere (1) in Table I at three different densities: (a) 0.10, (b) 0.50, and (c) 1.00 g/l.

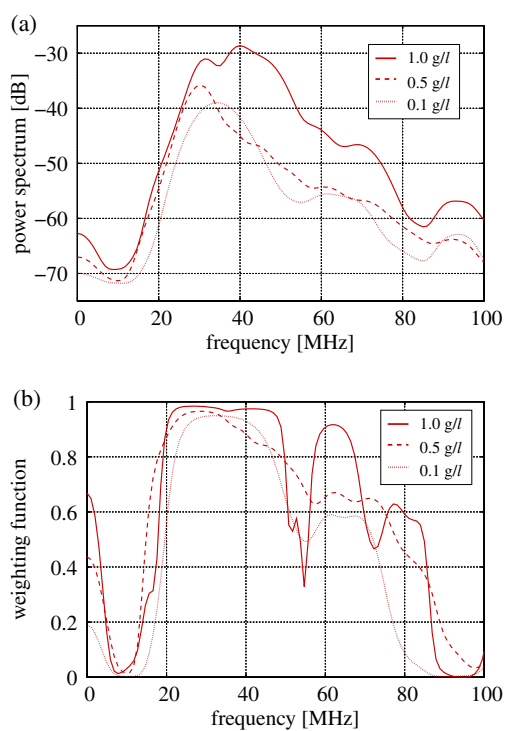


Fig. 13. (Color online) (a) Power spectra $P_s(f)$ of the ultrasonic echoes from the microsphere (1) in Table I obtained at different densities of microspheres mixed with water. (b) Weighting functions $w(f_k)$ obtained from MSCF among the ultrasound echoes scattered from microsphere (1) in Table I for each density of microspheres.

considered. On the other hand, as shown in Fig. 13(b), the weighting functions $w(f_k)$ show large values between 50 and 90 MHz regardless of the density of microsphere. Therefore, the influence of multiple scattering are not a dominant reason on the difference between the weighting functions $w(f_k)$ in basic experiments and *in vivo* experiments. Figure 14 shows RF echoes scattered from microspheres (blue line) and from RBCs (red line) in the lumen. As shown in Fig. 14, the main reason for the difference of weighting

functions $w(f_k)$ is considered to be the strong scattering of microspheres because the MSCF was used as the weighting function $w(f_k)$ and the SNR of the echoes, which is evaluated by the MSCF, obtained from microspheres are larger than that of echoes from RBCs in the lumen of the vein. The difference of acoustic impedance between microspheres and RBCs should be further considered in the future work.

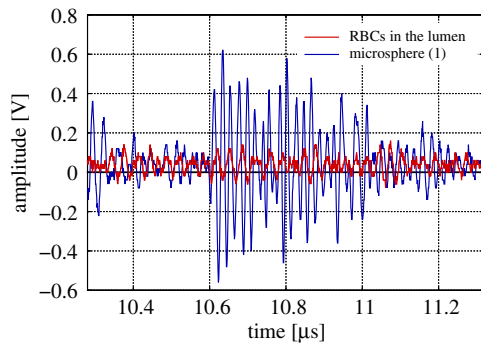


Fig. 14. (Color online) RF echoes scattered from RBCs in the lumen of the vein and the microsphere (1) in Table I.

In the *in vivo* experiments with avascularization, the averaged estimated diameters (12–22 μm) of RBCs during avascularization were larger than the diameters (4–8 μm) at rest and after recirculation. However, the normalized power spectra $\log_{10} P_s(f)/P_r(f)$ are strongly affected by dips in measured power spectra $P_r(f)$ with interference obtained by RF echoes from same position at the posterior wall.

This means that the luminal and external surfaces of the posterior wall of the vein included in the window width for frequency analysis are positioned so that it is thought that dips in measured normalized power spectrum $\log_{10} P_s(f)/P_r(f)$ are occurred from the interference of particular echoes reflected from the luminal and external surfaces of the posterior wall. Therefore, to reduce the influences of dips in power spectrum, it is necessary to acquire echoes obtained from only the luminal surface of the posterior wall of the vein included in the window width for frequency analysis.

In the present study, RF echoes scattered from RBCs in the lumen of the vein are acquired from only the focal point, and spatial distribution of scatterer sizes in the radial direction of vein have not been estimated. As shown in Fig. 11, the change in brightness occurred in the radial direction of the lumen of the vein suggested that the scatterer diameters of aggregated RBCs arisen from avascularization are spatially inhomogeneous.

Although there are still many factors to be investigated such as acoustic impedance of microspheres and influences of dips in power spectra, the results of the present study show the possibility of utilizing the proposed method for the noninvasive assessment of RBC aggregation.

Acknowledgment

We would like to thank Tomey Corporation for its cooperation on the use of the diagnostic equipment.

- 1) K. Tuzuki, H. Hasegawa, and H. Kanai: *Jpn. J. Appl. Phys.* **47** (2008) 4180.
- 2) K. Ikeshita, H. Hasegawa, and H. Kanai: *Jpn. J. Appl. Phys.* **48** (2009) 07GJ10.
- 3) D. G. Paeng, R. Y. Chiao, and K. K. Shung: *Ultrasound Med. Biol.* **30** (2004) 815.
- 4) N. Saitoh, H. Hasegawa, and H. Kanai: *Jpn. J. Appl. Phys.* **48** (2009) 07GJ08.
- 5) C. C. Huang and S. H. Wang: *Jpn. J. Appl. Phys.* **45** (2006) 7191.
- 6) K. Ujiie: *Chimmoku no Kessen* (Silent Clots: Life's Biggest Killers) (Chuo Art Publishing, Tokyo, 2000) [in Japanese].
- 7) S. Oka: *Reoroji —Seibutu Reoroji—* (Rheology —Biorheology—) (Chuo Publishing, Tokyo, 1974) [in Japanese].
- 8) M. Sugawara and N. Sugawara: *Ketsueki no Reoroji to Ketsuryu* (Rheology of Blood and Blood Flow) (Corona Publishing, Tokyo, 2003) [in Japanese].
- 9) A. Chabanel, M. H. Horellou, J. Conard, and M. M. Samama: *Br. J. Haematol.* **88** (1994) 174.
- 10) S. Berliner, D. Zeltser, R. Rotstein, R. Fusman, and I. Shapira: *Med. Hypotheses.* **57** (2001) 207.
- 11) H. Schmid-Schönbein and E. Volger: *Diabetes* **25** (1976) 897.
- 12) S. M. Razavian, V. Atger, Ph. Giral, M. Cambillau, M. Del-Pino, A. C. Simon, M. Moatti, and J. Levenson: *Arterioscler. Thromb.* **14** (1994) 361.
- 13) Y. Kikuchi, K. Sato, and Y. Mizuguchi: *Microvasc. Res.* **47** (1994) 126.
- 14) D. G. Paeng, K. H. Nam, and K. K. Shung: *Ultrasound Med. Biol.* **36** (2010) 1118.
- 15) D. G. Paeng, K. H. Nam, M. J. Choi, and K. K. Shung: *IEEE Trans. Ultrason. Ferroelectr. Freq. Control* **56** (2009) 880.
- 16) E. Franceschini, F. T. H. Yu, and G. Cloutier: *J. Acoust. Soc. Am.* **123** (2008) EL85.
- 17) E. Franceschini, F. T. H. Yu, F. Destrempes, and G. Cloutier: *Proc. IEEE Ultrasonics Symp.*, 2009, p. 301.
- 18) F. L. Lizzi, M. Astor, A. Kalisz, T. Liu, D. J. Coleman, R. Silverman, R. Ursea, and M. Rondeau: *Proc. IEEE Ultrasonics Symp.*, 1996, p. 1155.
- 19) F. T. H. Yu and G. Cloutier: *J. Acoust. Soc. Am.* **122** (2007) 645.
- 20) P. M. Morse and H. Feshbach: *Methods of Theoretical Physics* (McGraw-Hill, New York, 1953).
- 21) M. F. Insana, R. F. Wagner, D. G. Brown, and T. J. Hall: *J. Acoust. Soc. Am.* **87** (1990) 179.
- 22) M. Ueda and Y. Ozawa: *J. Acoust. Soc. Am.* **77** (1985) 38.
- 23) I. Fontaine and G. Cloutier: *J. Acoust. Soc. Am.* **113** (2003) 2893.
- 24) F. L. Lizzi, M. Greenebaum, E. J. Feleppa, M. Elbaurn, and D. J. Coleman: *J. Acoust. Soc. Am.* **73** (1983) 1366.
- 25) E. J. Feleppa, F. L. Lizzi, D. J. Coleman, and M. M. Yaremko: *Ultrasound Med. Biol.* **12** (1986) 623.
- 26) H. Kanai: *Oto-Shindo no Supekutoru Kaiseki* (Spectrum Analysis of Sound and Vibration) (Corona Publishing, Tokyo, 1999) [in Japanese].
- 27) S. Miwa: *Sekkekkyu* (Red Blood Cell) (Igaku-Shoin, Tokyo, 1998) [in Japanese].
- 28) S. Yagi and K. Nakayama: *Nihon Onkyo Gakkaishi* **39** (1983) 659 [in Japanese].
- 29) S. Yagi and K. Nakayama: *Nihon Onkyo Gakkaishi* **43** (1987) 777 [in Japanese].